JOURNAL OF PROPULSION AND POWER
Vol. 21, No. 2, March–April 2005

Theoretical Prediction of Resonance in Nozzle Flows

Henry Y. W. Wong*
ESA, European Space Research and Technology Center, 2200AG Noordwijk, The Netherlands

Resonance and damping in the shock movement induced either by a low-pressure ratio in a transonic convergent–divergent nozzle flow or by a supersonic or hypersonic flow in an overexpanded nozzle subject to external pressure fluctuations have been studied experimentally and numerically in the past. The underlying mechanisms for this resonance phenomenon in both cases are not fully understood. A perturbative quasi-one-dimensional model, coupled with a dual-oscillator concept, is given to explore the physical parameters that govern the shock excursion and the wave transport in the subsonic domain downstream of the shock. It is shown that the standing wave (strong resonance) in the former case is a consequence of superimposing two almost identical in amplitude but in opposite direction traveling waves through the subsonic domain inside the separated boundary layer. In the latter case, a relatively weak resonance is encountered as a result of the phasing in the convective energy transported between the energy dissipation due to the shock movement and the energy supply due to external pressure fluctuations. Resonant frequencies and pressure fluctuations compare well with the available experimental data and numerical solutions.

Nomenclature

A^*, A	=	throat and local cross-sectional area
a	=	speed of sound
c, $c_{\max}$	=	shock velocity and its maximum speed
c_p	=	specific heat capacity at constant pressure
c_r, c_r'	=	local Riemann characteristic speed and its streamwise derivative
c_w	=	wave speed
d	=	geometrical factor
E	=	acoustic reflection parameter
E_{s1}, E_{s2}, E_c	=	stored and convective energies
e	=	internal energy per unit mass
f, λ	=	frequency and wavelength
L	=	distance between shock and exit
M	=	Mach number
m, $\dot{m}$	=	mass flow and mass flow rate
P, P_T	=	static and total pressures
r^*	=	throat radius
T	=	static temperature
t	=	time
u	=	local flow velocity
x	=	displacement relative to shock mean location
Y, Y', Y''	=	acoustic admittance and its streamwise derivatives
γ	=	ratio of specific heat capacities
ε, ε_a, ε_b	=	perturbation parameters
θ	=	cone angle relative to its symmetry axis
κ, κ_d	=	wave numbers
ξ	=	phase angle between traveling waves
ρ	=	flow density
ϕ	=	phase angle between shock motion and pressure behind shock
ψ	=	phase angle between pressure behind shock and pressure at exit
ω	=	angular frequency

Subscripts

m	=	maximum modulus value
0	=	mean or steady value
1, 2	=	upstream and downstream of shock
3	=	nozzle exit

Received 12 December 2003; revision received 30 June 2004; accepted for publication 17 July 2004.

*Senior Consultant, Advanced Operations and Engineering Services; henry.wong@aoes.nl. Member AIAA.

I. Introduction

RESONANCE phenomenon in nozzle flows has been studied in the past by many researchers not only because of academic interest, but also of its significance in many engineering applications ranging from mixing,[1] jet noise control[2] to buffeting in external flows[3] and rocket engine instability.[4,5] For instance, in the case of convergent–divergent nozzles without any abrupt change in the cross-sectional area under a transonic flow condition at a pressure ratio much lower than the design value, flow separation takes place just downstream of the throat shock. Consequently, resonance and tones are encountered with such a nozzle flow condition. Research has been conducted experimentally,[6–8] as well as numerically.[7,9] An excellent overview of this activity has been reported by Zaman et al.[6]

In the case of supersonic or hypersonic cold subscaled rocket nozzle flows, such as those described by Schwane et al.,[4] flow separation takes place just downstream of a separation shock, the so-called free shock separation (FSS), located somewhere between the throat and the nozzle exit inside the overexpanded nozzle, depending mainly on the pressure ratio. A relatively more complex flowfield, the so-called restricted shock separation (RSS), can arise if the flow separation reattaches to the nozzle wall downstream of the initial separation location. A detailed account on the flow separation concept related to the side-load behavior of this kind of nozzle can be found by Terhardt et al.[10] Under this cold flow condition, where the movement of the separation shock in the FSS mode is under the influence of external pressure fluctuations at the nozzle exit, amplification of fluctuating pressure correlations between the region downstream of the separation shock and the external flow has been reported and studied experimentally[11] and numerically.[4] The shock excursion of this kind of shock movement, which depends on this amplification factor, has a great influence on the side-load effect to the nozzle in the case where the flow separation is asymmetric under certain conditions and may pose a threat to the occurrence of structural fatigue of nozzles.

There are other kind of nozzle flows where resonance phenomenon can be encountered such as those studied by Hill and Greene[1] and Hussain and Hasan[12] in which the nozzle has an abrupt change in the cross-sectional area, sometimes known as whistler nozzles. We shall confine our study to the case without any abrupt area change. Another area that is beyond the scope of this study involves a complex interference of tones generated by interactions between disturbances initiated at the nozzle lip and the shear layer

at the exit of an underexpanded supersonic jet flow. This induces a resonance phenomenon commonly known as screech tones, as reported by Krothapalli and Hsia.[2]

In all cases, a literature survey of all the available journals and proceedings published internationally shows that analytical study in the resonance phenomena in nozzle flows is almost nonexistent, which indicates the degree of complexity in the flowfield involved. In fact, the mechanism involved in the generation of the resonance phenomena, ranging from transonic to hypersonic nozzle flows as mentioned earlier, hitherto is still not fully understood.

An analytical relationship between the shock movement and its downstream pressure was first derived by Tijdeman[13] for a transonic flow around oscillating aerofoils with an assumption of Mach number freeze. Culick and Rogers[14] have presented a useful analysis in the response of a normal shock inside a divergent channel at low frequencies, but without going further into the resonance phenomenon. Sajben[15] has further extended the results of Culick and Rogers[14] for a higher frequency. These results will be useful as a cross-check with some of the results presented here.

The present study demonstrates an analytical approach to solve the interaction between a fluctuating external pressure at the exit of a conical nozzle and the conical shock induced by the pressure ratio inside the nozzle. The main objective is to understand the physical phenomena, mainly inviscid, governing the shock excursion and the wave transport in the subsonic region downstream of the shock, which have a significant influence on the mechanism in the generation of a standing wave within the subsonic domain inside the nozzle.

There are some flow similarities between the convergent–divergent nozzle and the conical nozzle cases. First, the pressure at the nozzle exit fluctuates periodically at resonance as demonstrated by the computational fluid dynamics (CFD) analysis shown by Loh and Zaman.[9] Second, there is a periodic shock movement. Third, the region downstream of the shock is subsonic. The main difference is the Mach number upstream of the shock in which one is transonic, and the other is supersonic or hypersonic. Basically, it is this difference that differentiates the amplitude of resonance, as shown in this study.

Moreover, the conical nozzle case is an approximation to the rocket nozzle case where a separation shock exists as mentioned earlier. It will be shown in this study how to modify this conical nozzle result and apply it to the rocket nozzle condition, such as the contoured S6 nozzle described by Torngren.[11]

This study forms a basis to interpret available experimental data, as well as to improve the design of experimental investigation in the area of an induced-shock movement inside a nozzle under the influence of external pressure fluctuations at the nozzle exit. In addition, this study provides a parametric investigation on the cause of resonance and the damping on the shock movement and a theoretical prediction of the shock excursion including its applicability to contoured nozzles.

This paper will introduce a perturbative quasi-one-dimensional inviscid theory for unsteady conical nozzle flows in two parts. The first part is to present a dual-oscillator concept governed by a one-dimensional wave transport equation that predicts the pressure fluctuation just downstream of the shock in relation to the external pressure fluctuation at the nozzle exit. The physical meaning of this simple one-dimensional wave equation in terms of resonance and damping will be explained, and the conditions of resonant frequencies at different harmonics will be derived. A comparison with the available experimental data[6,8] is included.

The second part is to model the conical shock movement as a consequence to the pressure fluctuation just downstream of the shock. A more rigorous quasi-one-dimensional nonlinear transport equation will be employed in the subsonic domain downstream of the shock, and its predictions based on the principle of energy conservation applied within a control volume will be compared with CFD results and with those from the first part of this study.

Finally, the range of applicability will be discussed, and an example of its application to a contoured S6 nozzle is provided and compared with the experimental data.[11]

II. Quasi-One-Dimensional Theory

A. Dual-Oscillator Concept

Consider a periodic motion of the conical shock induced by external pressure fluctuations at the end of the nozzle as shown in Fig. 1.

The external fluctuating pressure behaves like an oscillator at one end of an elastic spring, sending mechanical longitudinal waves to the other open end of the spring, where a periodic shock motion (linear oscillator) is induced. These oscillators are correlated but not necessarily in phase, and if there is a wave reflection from a subsonic domain upstream of the shock, to be justified, the effect of the combination of these longitudinal waves could create a standing wave. We shall examine under what conditions that a standing wave can be created inside the subsonic domain between the conical shock and the nozzle exit.

The first step is to establish a simple wave transport equation between the two oscillators: the periodic shock motion and the external fluctuating pressure. A more rigorous quasi-one-dimensional nonlinear transport equation will be presented in the second part of this theory. Consider a one-dimensional wave equation,

$$\frac{\partial^2 \Delta P}{\partial \boldsymbol{x}^2} = \frac{1}{c_w^2}\frac{\partial^2 \Delta P}{\partial t^2} \tag{1}$$

where c_w, for a wave traveling upstream towards the shock, can be defined as

$$c_w = \omega/\kappa = a - \boldsymbol{u}_0 \tag{2}$$

and for a wave traveling downstream toward the nozzle exit can be defined as

$$c_w = \omega/\kappa_d = a + \boldsymbol{u}_0 \tag{3}$$

ΔP is the fluctuating component of the local static pressure in the subsonic domain. A solution to Eq. (1) is sought subject to two boundary conditions. The first boundary condition is the periodic pressure fluctuation just downstream of the shock, which can be written as, at $\boldsymbol{x} = 0$,

$$\Delta P = \varepsilon_{20} P_{20} \sin(\omega t) \tag{4}$$

(Note that it is relatively easier to comprehend the physical meaning of the equation in terms of a trigonometric function than of a complex function e^{iwt}, which most acoustic scientists employ. The mathematical advantage of using a complex function to represent a periodic variation is appreciated.[16,17])

The second boundary condition is the external fluctuating pressure at $\boldsymbol{x} = L$ and can be written as

$$\Delta P = \varepsilon_{30} P_{30} \sin(\omega t + \psi) \tag{5}$$

where $\varepsilon_{30} P_{30}$ is just a fraction of the mean static pressure P_{30}.

A general solution to Eq. (1) is

$$\Delta P = \varepsilon_a \sin(\omega t + \kappa \boldsymbol{x}) + \varepsilon_b \sin(\omega t - \kappa_d \boldsymbol{x} + \xi) \tag{6}$$

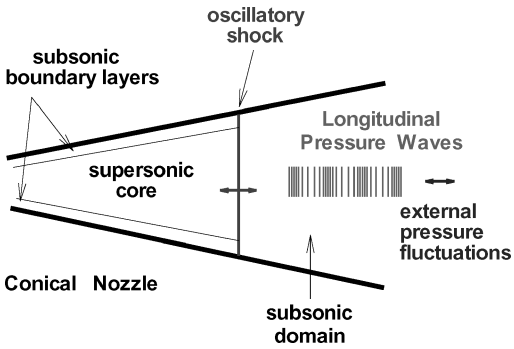

Fig. 1 Dual-oscillator concept.

Equations (4) and (6) yield

$$\varepsilon_a + \varepsilon_b \cos(\xi) = \varepsilon P_{20}, \qquad \varepsilon_b \sin(\xi) = 0 \tag{7}$$

Similarly, from Eqs. (5) and (6), we have

$$\varepsilon_a \cos(\kappa L) + \varepsilon_b \cos(\xi - \kappa_d L) = \varepsilon_{30} P_{30} \cos(\psi)$$

$$\varepsilon_a \sin(\kappa L) + \varepsilon_b \sin(\xi - \kappa_d L) = \varepsilon_{30} P_{30} \sin(\psi) \tag{8}$$

Equation (7) gives two possible solutions, $\varepsilon_b = 0$ or $\xi = n\pi$, where n is an integer. The first solution implies $\varepsilon = \varepsilon_{30}$ because, for a first-order approximation in the case of a small cone angle, $P_{20} \approx P_{30}$, which is just a steady solution. Substitution of the second solution into Eqs. (7) and (8) yields

$$\varepsilon_a \cos(\kappa L) \pm \varepsilon_b \cos(\kappa_d L) = \varepsilon_{30} \cos(\psi) P_{30}$$

$$\varepsilon_a \sin(\kappa L) \mp \varepsilon_b \sin(\kappa_d L) = \varepsilon_{30} \sin(\psi) P_{30}$$

$$\varepsilon_a \pm \varepsilon_b = \varepsilon P_{20} \tag{9}$$

Equation (9) yields an equation for the phase shift between the pressure just behind the shock and the external pressure at the nozzle exit,

$$\tan(\psi) = \frac{\varepsilon_a \sin(\kappa L) \mp \varepsilon_b \sin(\kappa_d L)}{\varepsilon_a \cos(\kappa L) \pm \varepsilon_b \cos(\kappa_d L)} \tag{10}$$

which is exactly the same result obtained by Culick and Rogers[14] with an acoustic complex analysis.

For a standing wave solution, this requires $\varepsilon_a = \varepsilon_b$, which is, from Eq. (9), equal to $\varepsilon P_{20}/2$. Substitution of this solution into Eq. (10) yields

$$\psi = [(\kappa - \kappa_d)/2]L + m\pi \tag{11}$$

where m is an integer. Substitution of Eq. (11) back into Eq. (9) yields

$$\varepsilon = \frac{\varepsilon_{30}(-1)^m}{\cos\{[(\kappa + \kappa_d)/2]L\}} \tag{12}$$

and the local perturbative pressure as

$$\Delta P = \frac{\varepsilon_{30} P_{30}(-1)^m}{\cos\{[(\kappa + \kappa_d)/2]L\}} \sin\left(\omega t + \frac{\kappa - \kappa_d}{2}\boldsymbol{x}\right) \cos\left(\frac{\kappa + \kappa_d}{2}\boldsymbol{x}\right) \tag{13}$$

Equation (12) shows that ε varies with frequency, and the condition for a standing-wave resonance with an infinite amplitude (no damping) to take place is

$$\kappa + \kappa_d = (2m + 1)\pi / L \tag{14}$$

which, together with Eqs. (2) and (3), gives the resonant frequency (natural frequency) as

$$f = \frac{(2m + 1)\left(a^2 - \boldsymbol{u}_{30}^2\right)}{4aL} \approx \frac{a(2m + 1)}{4L} \approx \frac{f\lambda(2m + 1)}{4L} \tag{15}$$

where $\boldsymbol{u}_{30}$ is the mean velocity at the nozzle exit, which is in general much smaller than the local speed of sound a. Moreover, Eq. (15) shows that, for this undamped resonance to occur, the nozzle exit has to be approximately an odd multiple of a quarter-wavelength distance away from the conical shock,

$$L \approx (\lambda/4)(2m + 1) \tag{16}$$

At the lowest resonant frequency (first harmonic) where $m = 0$, $L \approx \lambda/4$. Resonance at a higher harmonic requires a longer L, as shown in Eq. (16). This simple analysis has shown the influence of the distance between the nozzle exit and the conical shock to the resonant frequency in the shock movement. This influence will be highlighted again in the more sophisticated analysis in the second part of this study.

We have established the necessary but not sufficient condition for a standing-wave resonance to occur based on the assumption that the one-dimensional wave transport equation is sufficient to represent the fluid dynamics in the subsonic domain. In fact, the one-dimensional wave equation is a linearized one-dimensional Euler equation by ignoring all of the nonlinear terms as shown by Lighthill.[18] This kind of linearization may not be appropriate if there exists a strong mean flow in the subsonic domain. In the second part of this study, we shall solve a quasi-one-dimensional Euler equation including all of the nonlinear terms. It will be shown that some of these nonlinear terms create damping effects to attenuate the shock movement and will be validated by CFD results. In other words, the one-dimensional wave equation removes all of the damping effects from the flowfield in the subsonic domain, and the amplitude of the damping depends very much on the energy in the mean flow relative to the energy in the wave.

In addition, a standing wave requires $\varepsilon_a = \varepsilon_b$, as shown in the theory that implies a strongly reflected downstream traveling wave superimposed on the upstream traveling wave in the subsonic domain. In the case of a supersonic or hypersonic nozzle flow, it will be shown in the second part of this study that a conical nozzle with a small cone angle results only a weakly reflected downstream traveling wave. These two factors, damping and wave reflectivity, attenuate significantly the magnitude of the standing-wave resonance in the subsonic domain.

However, in the case of a transonic nozzle flow, such as those described by Zaman et al.,[6] and Sajben and Kroutil,[8] the strongly reflected traveling wave solution gives a reasonable prediction for the resonant frequencies. Table 1 summarizes a comparison between the experimental data and the theory. Because the mean velocity $\boldsymbol{u}_{30}$ at the nozzle exit and the shock location are not available in Refs. 6 and 8, only the upper bound frequency is theoretically predicted in each case, as shown in Table 1. L can only be approximated to be the distance between the throat and the nozzle exit. Some of the experimental data have been confirmed by CFD prediction, as reported by Loh and Zaman.[9] The range in the experimental data comes from the increment of the pressure ratio between the plenum and the ambient pressures for the case of Zaman et al.,[6] or from the different levels of inlet blockage due to the thickness of the boundary layer for the case of Sajben and Kroutil.[8] In general, the range shows that the resonant frequency increases as the pressure ratio increases. In theory, as the pressure ratio increases, the onset of the separated boundary layer takes place at a location farther downstream away from the throat; hence, L is smaller according to our definition of L. The separated boundary layer stays relatively closer to the nozzle wall with a lower mean velocity $\boldsymbol{u}_{30}$ in the subsonic domain inside the boundary layer. From Eq. (15), this implies that the resonant frequency is larger, which is consistent with the trend of the experimental data.

It can be seen that two of the nozzles have a range of resonant frequencies above the corresponding maximum theoretical value. These nozzles are designed to have a half-angle of divergence of less than 2 deg, which is a three-dimensional effect on the resonant frequency that can be ignored. The small divergence angle, coupled

Table 1 Comparison between theory and experimental data in resonant frequency

Nozzle	Throat-exit length L^*, m	Divergence angle θ, deg	Resonant frequency, f_r, kHz	
			Experiment	Theory
2T2[a]	0.038	1.83	2–5	2.2
5T1[a]	0.107	6.35	0.3–0.6	0.8
6T2[a]	0.019	0.76	4–7	4.5
1T1[a]	0.0095	8.34	3–5	8.9
McDonnell Douglas[b]	0.551	8.8	0.1–0.13	0.15

[a]NASA John H. Glenn Research Center convergent–divergent three-dimensional nozzle (Zaman et al.[6]).
[b]Two-dimensional diffuser (Sajben and Kroutil[8]).

with a progressively thicker viscous boundary layer downstream, provides a flow condition that could delay the shock formation at the throat to a location much farther downstream away from the throat. In addition, if the boundary layer is turbulent and its thickness is developed or changed significantly within a short streamwise length scale, a strong acoustic wave reflection could take place there instead of at the exit. As a result, the length parameter for the subsonic wave transport, L, is much smaller than the distance between the throat and the exit, L^*, which implies a larger resonant frequency according to Eq. (15).

With a larger angle of divergence, the viscous effect has less influence on both the shock formation at the throat and the subsonic wave propagation through the separated boundary layer outside the viscous sublayer.

Moreover, in addition to the viscous effect, there are other effects that can damp out or attenuate the amplitude of resonance. These effects will be discussed in the second part of this study.

It is important to understand the mechanism of creating a standing wave inside a nozzle to explain why a standing-wave resonance can occur only in a low supersonic or transonic flow condition, but tends to be attenuated in a high supersonic flow condition as indicated by the experimental data.[6,11]

As discussed by Zaman et al.,[6] a feasible mechanism is that the separated boundary layer downstream of the shock supports the growth of the wave instability inside the subsonic domain. Another mechanism is related to the longitudinal acoustic resonance within the subsonic domain. The wave instability along the separated boundary layer induces longitudinal as well as transverse waves inside the subsonic domain. However, it is only the longitudinal wave that can contribute to the mechanism of generating acoustic resonance. Because of the discontinuity in the boundary condition at the nozzle exit, any subsonic downstream travelling longitudinal wave initiated from the separation shock has a reflection at the exit and travels back upstream through the subsonic stems of the shock. However, contrary to Zaman et al.,[6] this upstream traveling wave does not reflect at the stems of the shock but continues to propagate upstream through the subsonic domain, upstream of the shock, until a reflected wave takes place ideally at the plenum, upstream of the throat, for a nozzle with a small cone angle. In practice, a reflected wave can be generated downstream of the plenum depending on the nozzle admittance as well as the local boundary layer development, which will be discussed further later. These azimuthal coherent reflected waves, after traveling through the upstream annular subsonic boundary layer, merge together to form one strongly reflected wave just downstream of the shock. This strongly reflected downstream traveling wave is then interfered with by the upstream traveling wave from the exit. It is this kind of superposition of the two, almost identical in amplitude but in opposite direction, traveling waves that creates the standing wave with multiple nodes and antinodes, including one pressure antinode at or close to the shock and a node close to the exit. The distance between a node and an antinode depends very much on the resonant frequency.

In the transonic or low supersonic flow condition, the subsonic domain inside the boundary layer is large enough to accommodate these acoustic traveling waves creating azimuthal coherent downstream traveling waves to interfere with the upstream traveling waves from the exit. In the high supersonic flow condition, the subsonic domain inside the boundary layer upstream of the shock is too small to allow the existence of acoustic coherent waves. The viscous sublayer damps out or attenuates significantly the amplitude of the acoustic waves. For this reason, any disturbance in the boundary layer upstream or downstream of the shock has a significant influence on the existence of or damping to the resonance phenomenom inside the nozzle.

According to the conservation of linear momentum, a totally reflected wave can be generated only if there exists a momentum from the shock to the acoustic wave equivalent to two times the magnitude of the momentum from the wave to the shock. Because any subsonic disturbance downstream of the shock can not travel upstream through the supersonic domain for a reverse in momentum, it is, therefore, not probable to have a strong wave reflection at the shock surface in the case where upstream of the shock is a supersonic flow. This supports the proposed mechanism that the acoustic wave downstream of the shock has to propagate through the subsonic domain close to the wall upstream of the shock for a strong wave reflection to take place.

Other effects such as the curvature of shock and multishock dissipation could play a role in the damping of the resonance phenomenom but will not be discussed further.

B. Induced Shock Motion

We begin the second part with a shock motion induced by a pressure fluctuation downstream of the shock. This forms the upstream boundary condition of the subsonic domain, downstream of the shock, which will be analyzed with the principle of energy conservation. Because of the approximation involved, most of the results shown in this part of the study are valid only for supersonic or hypersonic flows where $M_1^2 \gg 1$.

Consider a periodic pressure fluctuation just downstream of the conical shock with an amplitude of εP_{20}. The pressure downstream of the shock can be given as, according to Eq. (4),

$$P_2 = P_{20}[1 + \varepsilon \sin(\omega t)] \tag{17}$$

An induced periodic motion of the shock can then be approximated by a simple harmonic motion with a displacement of the shock $\Delta \boldsymbol{x}$ about its mean location $\boldsymbol{x}_0$ written as

$$\Delta \boldsymbol{x} = -\Delta \boldsymbol{x}_m \sin(\omega t + \phi) \tag{18}$$

The negative sign means that $\Delta \boldsymbol{x}$ decreases with an increase of P_2. The shock velocity is, therefore, given by

$$\boldsymbol{c} = -\omega \Delta \boldsymbol{x}_m \cos(\omega t + \phi) \tag{19}$$

At a finite frequency with the shock speed c assumed to be of the order ε, which can be confirmed a posteriori in the solution, hence at any time during the motion, $c \ll u_1$ or u_2. Under this condition, one can transform this unsteady problem into a steady one by a Galilean transformation where the flow velocity is relative to the shock velocity $\boldsymbol{c}$. The continuity, momentum, and energy equations become

$$\rho_1(\boldsymbol{u}_1 - \boldsymbol{c}) = \rho_2(\boldsymbol{u}_2 - \boldsymbol{c}) \tag{20}$$

$$P_1 - P_2 = \rho_1(\boldsymbol{u}_1 - \boldsymbol{c}) \cdot (\boldsymbol{u}_2 - \boldsymbol{u}_1) \tag{21}$$

$$c_p T_1 + (\boldsymbol{u}_1 - \boldsymbol{c})^2 \big/ 2 = c_p T_2 + (\boldsymbol{u}_2 - \boldsymbol{c})^2 \big/ 2 \tag{22}$$

At a very high frequency such as 500 Hz for the conical nozzle test case condition to be shown later, the acceleration effect in the shock motion becomes significant, and the assumption $c \ll u_1$ may not be valid because the shock speed is approaching to the magnitude of $\boldsymbol{u}_1$. The range of frequency considered for the validation of this test case is from 0 to 200 Hz.

Solving these equations to a first-order approximation in terms of $\boldsymbol{c}/\boldsymbol{u}_{10}$ gives

$$M_2^2 = \frac{\gamma - 1}{2\gamma} + \frac{\gamma + 1}{\gamma} \frac{\boldsymbol{c}}{\boldsymbol{u}_{10}} + \mathcal{O}\left(\frac{\boldsymbol{c}^2}{\boldsymbol{u}_{10}^2}\right) \tag{23}$$

$$\frac{P_2}{P_1} = \frac{2\gamma M_1^2 - (\gamma - 1)}{\gamma + 1}\left(1 - \frac{2\boldsymbol{c}}{\boldsymbol{u}_{10}}\right) + \mathcal{O}\left(\frac{\boldsymbol{c}^2}{\boldsymbol{u}_{10}^2}\right) \tag{24}$$

as $M_1^2 \gg 1$. This shows the same result of the shock speed influence to the pressure ratio at the shock as reported by Nixon[19] and Tijdeman[13] for the analysis of unsteady transonic aerofoils. To connect the reservoir conditions to the supersonic flow just upstream of the shock, we employ from the standard formulas[20]

$$P_T/P_1 = \left\{1 + [(\gamma - 1)/2]M_1^2\right\}^{\gamma/(\gamma - 1)} \tag{25}$$

This problem is uniquely defined provided there is an equation to relate the geometry and the nozzle flow. For a quasi-one-dimensional nozzle, the area ratio is related to the supersonic Mach number just upstream of the shock,[20]

$$\boldsymbol{A}^*/\boldsymbol{A} = [(\gamma+1)/2]^{(\gamma+1)/2(\gamma-1)} \times M_1\left\{1+[(\gamma-1)/2]M_1^2\right\}^{-(\gamma+1)/2(\gamma-1)} \tag{26}$$

Substitution of Eqs. (17–19), (25), and (26) into Eq. (24) and posing a first-order perturbation for P_1 and M_1 in terms of ε yield the following set of shock movement equations:

$$\frac{\Delta \boldsymbol{x}}{\boldsymbol{x}_0} = \varepsilon\left(\frac{\boldsymbol{x}_0\tan\theta+\boldsymbol{r}^*}{d\boldsymbol{x}_0\tan\theta}\right)\underbrace{\left[\frac{-1}{M_{10}}+\frac{(\gamma+1)M_{10}}{2+(\gamma-1)M_{10}^2}\right]}_{\text{geometry (G)}} \times \underbrace{\left[\frac{2+(\gamma-1)M_{10}^2}{-2\gamma M_{10}}\right]}_{\text{reservoir (R)}}\underbrace{\left(\frac{\gamma+1}{2M_{10}^2-\gamma-3}\right)}_{\text{pressure behind shock (P)}}\frac{P_{20}}{P_{10}} \times \left[\sin(2\pi f t)-\underbrace{\frac{2}{\boldsymbol{u}_{10}}}_{\text{shock velocity}}\frac{2\pi f}{\varepsilon}\Delta\boldsymbol{x}_m\cos(2\pi f t+\phi)\right]+\mathcal{O}(\varepsilon^2) \tag{27}$$

$$\frac{\Delta \boldsymbol{x}_m}{\boldsymbol{x}_0} = -\varepsilon\cos(\phi)(\text{GRP})+\mathcal{O}(\varepsilon^2) \tag{28}$$

$$\cos(-\phi) = 1\Big/\sqrt{\left\{(2\pi f)^2\left(\frac{2}{\boldsymbol{u}_{10}}\right)^2(\boldsymbol{x}_0\text{GRP})^2+1\right\}} \tag{29}$$

as $M_{10}^2 \gg 1$. Here d is a geometrical number for dimension with $d=2$ for three dimensions and $d=1$ for two dimensions. All of the unknowns with a subscript 0 are either given or steady variables that can be calculated from the standard formulas.[20] Equations (19), (28), and (29) show that the maximum speed of the shock is of the order ε as assumed, where

$$c_{\max} = 2\pi f\,\Delta\boldsymbol{x}_m = \varepsilon[\boldsymbol{u}_{10}\sin(-\phi)/2] \tag{30}$$

Equation (29) shows that the phase angle is independent of the amplitude of the pressure fluctuation and its asymptotic value is a phase lag of 90 deg. Furthermore, the magnitude of the shock motion decreases inversely proportional to frequency. These are exactly the same results as in the transonic periodic shock oscillations on a rigid airfoil based on transonic potential theory.[19] Based on these equations, one can plot the trajectory of the shock motion against the pressure variation in front of and behind the shock as shown in the CFD validation section.

C. CFD Validation for Induced Shock Motion

Geometry

A two- or three-dimensional (axisymmetric) conical nozzle is valid for this theory. For the benefit of a minimum computational cost, a two-dimensional conical nozzle is taken for the validation of the theory with inviscid calculations from CFD. To simulate the chamber and boundary conditions similar to the S6 contoured nozzle,[4,21] the conical nozzle is designed to have a length of 2.55 m with a conical shock at Mach 5.54 located at 1.9 m from the throat. The wall angle is 24.0 deg.

Test Case Conditions

The medium fluid is a perfect gas with a specific heat capacity ratio of 1.4. The chamber stagnation pressure is 21 bar. The stagnation temperature in the chamber is 300 K. The ambient pressure is 0.77 bar with a fluctuation of 4.5 and 9% of the ambient pressure in amplitude and a range of frequency of 2–208 Hz. The nozzle wall is assumed adiabatic and rigid in the computations.

Computational Grid

Coarse and fine grids are generated to find an optimal grid for time-accurate computations. In addition, a long grid is generated to extend the external boundary condition farther downstream to test its sensitivity to the solution.

Methodology

The numerical computations are performed with the time-accurate two- or three-dimensional Navier–Stokes CFD code EURANUS, developed by the Aeronautical Research Institute of Sweden FFA.[22] Different numerical schemes are available; in the present computations, the symmetric Harten/Yee scheme has been used for its ability to resolve shocks, shear layers, and boundary layers with high accuracy. The time integration is fully implicit coupled with a multigrid accelerated Runge–Kutta scheme for the convergence of a solution to a new time level employing the pseudotime approach.[23] The accuracy of this code in the prediction of unsteady aerodynamics for base buffeting has been validated.[24]

D. Results and Discussion

Figure 2 shows the shock excursion and the wall pressure variations inside the conical nozzle at a 2-Hz external pressure fluctuation.

The pressures just upstream and downstream of the conical shock compare well with the quasi-one-dimensional theory. This is a quasi-steady case, which gives an almost linear variation of the pressure behind shock at different locations in the cycle. This is repeated for a large range of frequencies, some of the results from which are shown in Figs. 3 and 4. Some of the CFD results presented here have been reproduced by another CFD code with different numerical schemes.[4]

Similar to the pressure distribution shown by Sajben,[15] one can draw an ellipse for the variation of the pressure behind shock at each frequency as shown in Figs. 3 and 4. It can be seen the predictions from the theory match closely with the computations. The maximum shock excursion takes place at around 45 Hz. For this reason, we test grid convergence at this frequency, and the result shows a difference of less than 1% as shown in Fig. 3.

Figure 5 shows a summary of a comparison between the theory and CFD results. It consists of frequency vs the phase shift between the shock movement and the pressure fluctuation behind shock, the maximum shock speed, and the maximum shock excursion. Figures 5a and 5b correspond to two different external pressure fluctuations, where ε_{30} are 0.09 and 0.045, respectively. At this stage, the variation of ε against frequency behind shock is provided by CFD simulations. However, it can be shown at a later stage that the comparison in the variation of ε against frequency between the results predicted by the theory and CFD shows good agreement. As shown in Fig. 5a, the fine grid solutions at 45 Hz are superimposed on the coarse grid solutions. The maximum discrepancy between the theory and CFD data is less than 15%, which takes place around the maximum pressure fluctuation with a value of ε around 0.25. Note again that this is a perturbation analysis, which is valid for a small perturbative parameter with a magnitude of around 0.10. To demonstrate this argument, the same set of computations is repeated with half of the external pressure fluctuation amplitude as shown in Fig. 5b.

Figure 5 shows that the parameter ε for the pressure fluctuation behind shock is finite at a resonant frequency (fundamental mode) of $\approx$50 Hz. However, based on the one-dimensional wave equation augmented with a strong standing wave, the prediction of the amplitude of ε is infinite at a resonant frequency (fundamental mode $m=0$) of around 150 Hz with $L=0.5$ m. This indicates that there is some kind of damping in the subsonic domain that is not covered by the one-dimensional wave equation as discussed earlier for the dual-oscillator concept. In the latter part of this study, it will be shown that the damping effect comes mainly from the interaction and correlation between the compressibility and the velocity in the subsonic domain that the one-dimensional linearized wave equation has neglected.

Furthermore, the strongly reflected wave model assumed in the standing wave solution may be incorrect for this kind of high supersonic or hypersonic nozzle flow. It will be shown that a weakly

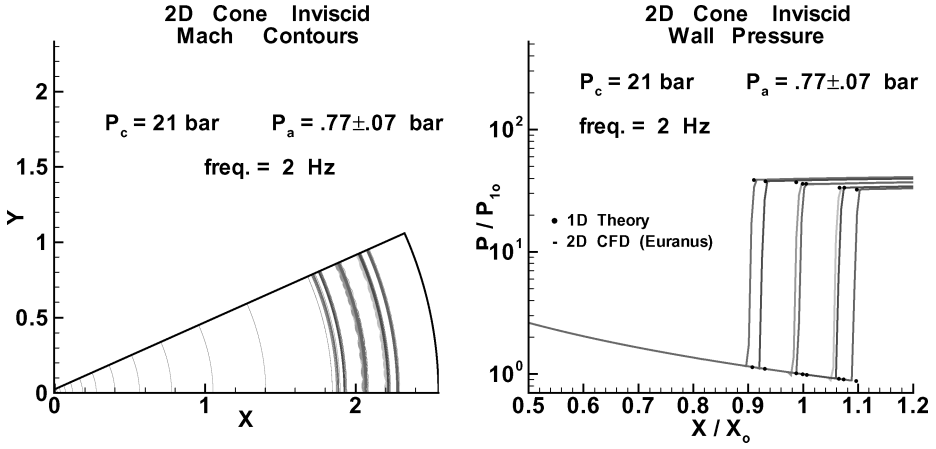

Fig. 2 Conical shock excursion and wall pressure at 2 Hz.

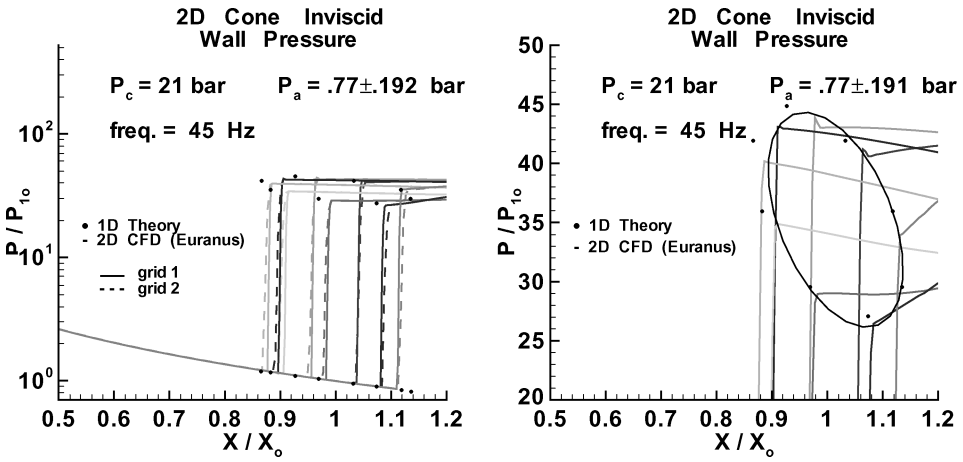

Fig. 3 Wall pressure variations at 45 Hz.

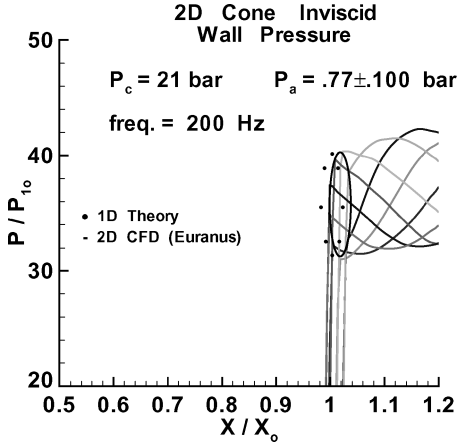

Fig. 4 Wall pressure variations at 200 Hz.

reflected wave model is a relatively more appropriate solution than the strongly reflected wave model. The strong acoustic standing-wave resonance is unlikely to take place but will be overcome by a relatively weak resonance as a result of the phasing in the convective energy transported between the energy dissipation due to the shock movement and the energy supply due to external pressure fluctuations.

III. Energy Conservation Principle

The principle of energy conservation is applied to balance the energy contributions over a cycle period from convection, external pressure work, and storage in the control volume, as shown in Fig. 6.

The control volume partially covers the supersonic flows, upstream of the conical shock, and the whole domain of the subsonic flows, downstream of the shock, down to the nozzle exit. At the nozzle exit, there is external pressure work (mechanical) against the subsonic flows. In addition, an energy exchange due to mass transfer (convection) takes place across the control surfaces at both the inlet and outlet of the control volume. Stored energy in the control volume consists of two parts. The first part considers the energy dissipation as a result of the periodic shock movement (linear oscillator). The second part considers the energy storage and dissipation in the subsonic flows as a result of the wave transfer between the shock and the external pressure at the nozzle exit. In fact, this is the part that requires the solving of the perturbed unsteady continuity and momentum equations, from which the energy based on the interactions among the local pressure, density, and velocity at the nozzle exit can be evaluated. It will be shown that these interactions at the exit form the core ingredient for the existence of resonance in the subsonic domain. Heat exchange through thermal conduction is not considered in this inviscid flow condition. The solid wall is assumed rigid and in an adiabatic condition. We shall consider the perturbative energy contribution from each form of the energy exchanges mentioned for one cycle period. Most of the perturbative parameters are presented in first-order accuracy. However, second-order terms from each parameter, based on the linear oscillator hypothesis, have been taken into account in the integration for the perturbative energy assessment.

A. Energy Storage

Periodic Shock Motion

The energy dissipated by the periodic shock motion can be obtained from the energy supply just downstream of (behind) the

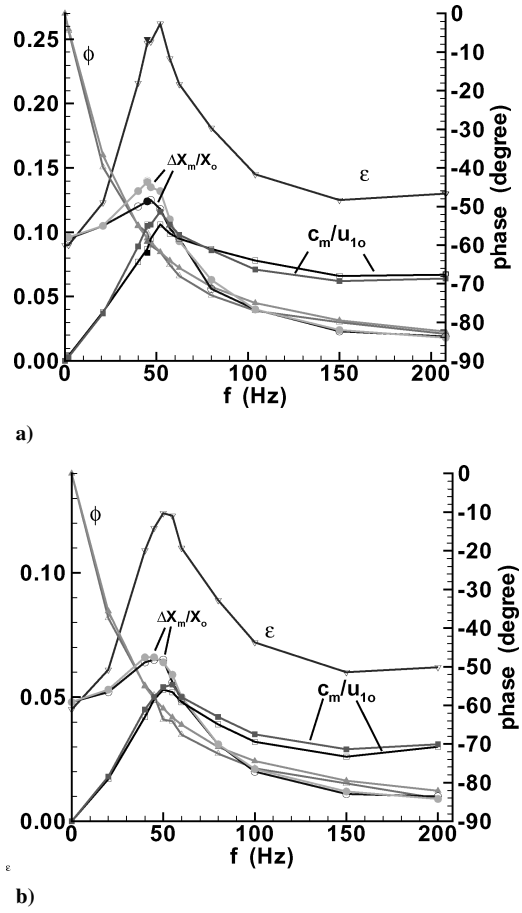

Fig. 5 Comparison between quasi-one-dimensional theory (filled symbols) and CFD: ▽, pressure amplitude %; △, phase; ○, shock displacement; and □, shock speed.

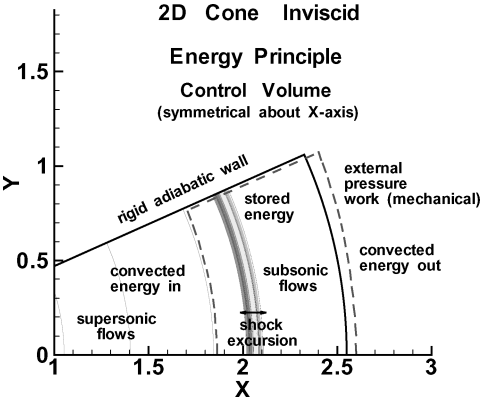

Fig. 6 Energy conservation principle.

shock, by integrating over a period the pressure work done across the shock,

$$\Delta E_{s1} = \int_0^{1/f} (P_1 - P_2)\boldsymbol{Ac}\,\mathrm{d}t \tag{31}$$

Posing the pressure and the Mach number as the sum of its mean and its perturbed component gives

$$P_1 = P_{10} + \Delta P_1, \qquad P_2 = P_{20} + \Delta P_2, \qquad M_1 = M_{10} + \Delta M_1 \tag{32}$$

Then substitution of Eqs. (17) and (32) into Eqs. (24) and (25) yields

$$\Delta P_1 = -P_{10}\frac{\gamma M_{10}\Delta M_1}{1 + [(\gamma-1)/2]M_{10}^2} + \mathcal{O}(\varepsilon^2) \tag{33}$$

$$\Delta P_1 = \frac{(\gamma+1)P_{20}}{\left[2M_{10}^2 - \gamma - 3\right]}\left[\varepsilon\sin(\omega t) + \frac{2\boldsymbol{c}}{\boldsymbol{u}_{10}}\right] + \mathcal{O}(\varepsilon^2) \tag{34}$$

Substitution of Eqs. (17–19), (32), and (34) into Eq. (31) leads to the energy dissipation,

$$\Delta E_{s1} = [8/(\gamma+1)]\pi^2\dot{m}_0 f(\Delta\boldsymbol{x}_m)^2 + \mathcal{O}\left[\left(\varepsilon^2/M_{10}^2\right), \varepsilon^3\right] \tag{35}$$

This is similar to the energy dissipated by a transverse string wave or a longitudinal spring periodic motion, $2\pi^2\dot{m}_0 f(\Delta\boldsymbol{x}_m)^2$. The difference in the coefficient is attributed to the correlation between the mass flow and the specific kinetic energy through the shock, which depends on the shock velocity, whereas in the longitudinal spring, the mass is a constant. Equation (35) shows that the perturbative stored energy is positive, which implies that some additional energy has been extracted from the dissipated energy due to the shock periodic motion and transferred to the convective energy downstream away from the shock.

Subsonic Domain

This is the second part of the energy storage contribution, which is essentially based on the variations of the static and dynamic pressures within this subsonic domain. To have a rigorous assessment on these two quantities, one has to solve the perturbed unsteady continuity and momentum equations as

$$\frac{\partial\rho}{\partial t} + \boldsymbol{u}\frac{\partial\rho}{\partial\boldsymbol{x}} + \rho\frac{\partial\boldsymbol{u}}{\partial\boldsymbol{x}} + \frac{\rho}{\boldsymbol{A}}\left(\frac{\partial\boldsymbol{A}}{\partial t} + \boldsymbol{u}\frac{\partial\boldsymbol{A}}{\partial\boldsymbol{x}}\right) = 0 \tag{36}$$

$$\frac{\partial\boldsymbol{u}}{\partial t} + \boldsymbol{u}\frac{\partial\boldsymbol{u}}{\partial\boldsymbol{x}} + \frac{\partial P}{\rho\partial\boldsymbol{x}} = 0 \tag{37}$$

Equations (36) and (37) are the general inviscid unsteady continuity and momentum equations for quasi-one-dimensional flows in which the cross-sectional area $\boldsymbol{A}$ can vary along the flow direction $\boldsymbol{x}$ as well as in time t (Refs. 18 and 25).

Let us start with the momentum equation by posing each of the local flow variables as the sum of its mean and its perturbed component so that

$$\rho = \rho_0 + \Delta\rho, \qquad \boldsymbol{u} = \boldsymbol{u}_0 + \Delta\boldsymbol{u}, \qquad P = P_0 + \Delta P \tag{38}$$

Substitution of Eq. (38) into Eq. (37) yields a first-order perturbed unsteady momentum equation,

$$\frac{\partial\Delta\boldsymbol{u}}{\partial t} + \frac{\partial(\boldsymbol{u}_0\Delta\boldsymbol{u})}{\partial\boldsymbol{x}} + \frac{\partial\Delta P}{\rho_0\partial\boldsymbol{x}} = \frac{\Delta\rho}{\rho_0^2}\frac{\partial P_0}{\partial\boldsymbol{x}} \tag{39}$$

However, from the isentropic flow relations,[20] the mean value (steady flow) of the density, pressure, and velocity in the subsonic domain can be expressed as

$$\frac{P_{20}}{P_{30}} = \left(\frac{\rho_{20}}{\rho_{30}}\right)^{\gamma} \tag{40}$$

$$\frac{\rho_{20}}{\rho_{30}} = \left(\frac{2 + (\gamma-1)M_{30}^2}{2 + (\gamma-1)M_{20}^2}\right)^{1/(\gamma-1)} \tag{41}$$

$$\frac{\boldsymbol{u}_{20}}{\boldsymbol{u}_{30}} = \frac{\rho_{30}\boldsymbol{A}_{30}}{\rho_{20}\boldsymbol{A}_{20}} \tag{42}$$

Because M_{20}^2 and M_{30}^2 are, in general, small quantities $\ll 1$, one can approximate these mean values to a good degree of accuracy as

$$\rho_{20} \approx \rho_{30}, \qquad \boldsymbol{A}_{20}\boldsymbol{u}_{20} \approx \boldsymbol{A}_{30}\boldsymbol{u}_{30}, \qquad P_{20} \approx P_{30} \tag{43}$$

Equation (43) implies that the perturbed unsteady momentum Eq. (39) is asymptotic to

$$\frac{\partial\Delta\boldsymbol{u}}{\partial t} + \frac{\partial(\boldsymbol{u}_0\Delta\boldsymbol{u})}{\partial\boldsymbol{x}} + \frac{\partial\Delta P}{\rho_{20}\partial\boldsymbol{x}} = 0 \tag{44}$$

The next step is to pose a general periodic solution for $\Delta \boldsymbol{u}$ that, for a wave traveling upstream towards the shock, can be of the form

$$\Delta \boldsymbol{u} = -[A\cos(\omega t + \kappa \boldsymbol{x}) + B\sin(\omega t + \kappa \boldsymbol{x})] \tag{45}$$

where the local speed of sound is given by

$$a = \omega/\kappa + \boldsymbol{u}_0 \tag{46}$$

or, for a wave traveling downstream toward the nozzle exit,

$$\Delta \boldsymbol{u} = -[C\cos(\omega t - \kappa_d \boldsymbol{x}) + D\sin(\omega t - \kappa_d \boldsymbol{x})] \tag{47}$$

where the local speed of sound is given by

$$a = \omega/\kappa_d - \boldsymbol{u}_0 \tag{48}$$

or a combination of both. The unknown constants A, B, C, and D can be found by satisfying the boundary conditions.

The velocity just behind the shock can be evaluated from the Galilean transformed continuity, momentum, and energy equations (20), (21) and (22), respectively, which yield

$$\boldsymbol{u}_2 = \frac{2\boldsymbol{c}}{\gamma+1} + \frac{\gamma - 1 + 2/M_{10}^2}{\gamma+1}\boldsymbol{u}_1 + \mathcal{O}\left(\frac{\varepsilon}{M_{10}^2}\right) \tag{49}$$

Substitution of $\boldsymbol{u}_2 = \boldsymbol{u}_{20} + \Delta \boldsymbol{u}_2$ and $\boldsymbol{u}_1 = \boldsymbol{u}_{10} + \Delta \boldsymbol{u}_1$ into Eq. (49) gives

$$\Delta \boldsymbol{u}_2 = 2\boldsymbol{c}/(\gamma+1) + \mathcal{O}\left(1/M_{10}^2, \varepsilon/M_{10}^2\right) \tag{50}$$

This is the upstream velocity boundary condition for $\Delta \boldsymbol{u}$.

For a wave traveling upstream toward the shock, Eq. (45), satisfying the upstream boundary condition Eq. (50), yields the coefficients

$$A = [2\omega/(\gamma+1)]\Delta \boldsymbol{x}_m \cos(\phi)$$

$$B = -[2\omega/(\gamma+1)]\Delta \boldsymbol{x}_m \sin(\phi) \tag{51}$$

and, similarly, for a wave traveling downstream toward the nozzle exit, the coefficients are

$$C = [2\omega/(\gamma+1)]\Delta \boldsymbol{x}_m \cos(\phi)$$

$$D = -[2\omega/(\gamma+1)]\Delta \boldsymbol{x}_m \sin(\phi) \tag{52}$$

In general, a feasible combination of the two traveling waves depends on the strength of the wave reflection inside the nozzle, which in turn determines the upstream condition at the nozzle exit. In the case of a strongly reflected wave traveling downstream, which can interact with or superimpose on the upstream traveling wave to form a standing wave, and if the resonant frequency is low, the streamwise length scale for the transition between the outflow condition just upstream of the nozzle exit and the downstream external flow condition could be significantly extended beyond the compact region[18] (which is the connection between the nozzle exit and the abrupt widened open space) at the nozzle exit. On the other hand, a weakly reflected wave traveling downstream cannot form a standing wave, and the superimposed wave is asymptotically close to the upstream traveling wave. The effect from the compact region in this case is, therefore, relatively insignificant to the flowfield inside the subsonic domain. In both cases, the amplitude of the wave depends on, among other things, the shock excursion length $\Delta \boldsymbol{x}_m$, which in turn depends on the frequency as well as the amplitude of the external pressure fluctuation. This indicates implicitly the influence of the downstream boundary condition on the solution of the acoustic wave propagation in the subsonic domain.

We shall consider the solutions of these two extreme cases and compare them with the corresponding numerical solutions from CFD, the same code employed and described in the validation section.

From Eqs. (45), (47), (51), and (52), the strongly reflected wave, superimposed on the upstream traveling wave, forms

$$\Delta \boldsymbol{u} = -[2\omega \Delta \boldsymbol{x}_m/(\gamma+1)]\cos\{\omega t + \phi + [(\kappa - \kappa_d)/2]\boldsymbol{x}\} \times \cos\{[(\kappa + \kappa_d)/2]\boldsymbol{x}\} \tag{53}$$

This is a standing-wave equation for the perturbed velocity with an amplitude varying with the location in the subsonic domain. Substitution of Eq. (53) into the perturbed momentum equation (44), subject to the boundary condition at the shock, Eq. (4), yields the perturbed pressure in the subsonic domain,

$$\Delta P = P_{20}\varepsilon \sin(\omega t) - [2\omega \Delta \boldsymbol{x}_m/(\gamma+1)]\rho_{20} a \sin \times \{\omega t + \phi + [(\kappa - \kappa_d)/2]\boldsymbol{x}\}\{[(\kappa + \kappa_d)/2]\boldsymbol{x}\}\sin \tag{54}$$

where a is the local speed-of-sound defined by Eq. (46) or (48).

Similarly, from Eqs. (45) and (51), the weakly reflected wave, superimposed on the upstream traveling wave, is asymptotic to

$$\Delta \boldsymbol{u} = -[2\omega \Delta \boldsymbol{x}_m/(\gamma+1)]\cos(\omega t + \phi + \kappa \boldsymbol{x}) \tag{55}$$

which is not a standing wave but traveling wave for the perturbed velocity with an amplitude independent of the location in the subsonic domain. Likewise, with a substitution of Eq. (55) into Eq. (44), subject to the boundary condition at the shock as given earlier, the corresponding perturbed pressure in the subsonic domain is

$$\Delta P = P_{20}\varepsilon \sin(\omega t) - [4\omega \Delta \boldsymbol{x}_m/(\gamma+1)] \times \rho_{20} a \sin[\omega t + \phi + (\kappa/2)\boldsymbol{x}]\sin[(\kappa/2)\boldsymbol{x}] \tag{56}$$

Both Eqs. (54) and (56) show that the amplitude of the perturbed pressure in the subsonic domain depends on the location inside the domain, which is a characteristic of a standing wave. Despite the significant differences in the perturbed velocity for each case, the resultant perturbed pressure shows similar behavior, but with a different phase and amplitude at each location in the subsonic domain. Compare ΔP from the Eqs. (54) and (56) with Eq. (13) from the one-dimensional wave equation crude approximation, which, together with Eq. (43), can be rewritten as

$$\Delta P = \varepsilon P_{20} \sin\{\omega t + [(\kappa - \kappa_d)/2]\boldsymbol{x}\}\cos\{[(\kappa + \kappa_d)/2]\boldsymbol{x}\} \tag{57}$$

It can be seen, as expected, that Eq. (57) is closer to the strongly reflected than to the weakly reflected wave solution. However, the phase angle ϕ is excluded in the crude approximation solution. This is attributed to the linearization in the continuity and momentum equations forming the one-dimensional wave equation, which is a crude approximation to this problem with a strong mean flow. The discarded nonlinear velocity terms remove the phase shift effect between the shock movement and the pressure behind the shock. At low frequencies, where $\phi \approx 0$ and all of the wave numbers are small, all of the solutions are approximately the same. It is reasonable to conclude that the one-dimensional wave equation crude approximation for this supersonic or hypersonic nozzle flow is still valid in a low-frequency range where the first term in Eqs. (54) and (56) dominates.

Moreover, if the mean velocity in the subsonic domain is small compared to the local speed of sound, which is usually the case particularly when viscosity is taken into account, $\kappa \approx \kappa_d$, the shock speed has to be low because it can not be larger than the local mean velocity behind the shock. As a result, the frequency is low, and the solution of the strongly reflected wave model, Eq. (54), is asymptotic to the linearized crude approximation, Eq. (57).

Now we focus back on the nonlinear solutions and compare them with the CFD solutions. In this way, we can understand better which model should be taken for further development in our analysis and what mechanism should be proposed a posteriori to fit with the model. The comparison follows the path of variation at different times of a cycle inside the subsonic domain for $\Delta \boldsymbol{u}$ and ΔP. Figure 7 shows the comparison in $\Delta \boldsymbol{u}$ at 45 Hz, and in ΔP at 200 Hz, with the weakly and the strongly reflected wave models.

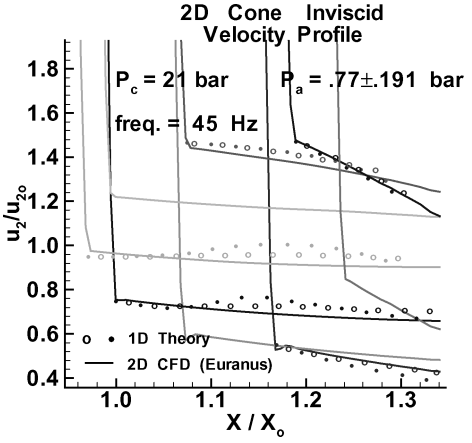

a) Velocity at 45 Hz

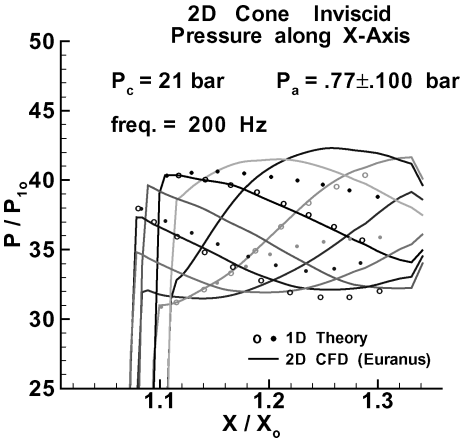

b) Pressure at 200 Hz

Fig. 7 Comparison of Δu and ΔP in wave models: ○, weakly reflected and ●, strongly reflected.

Both models show good agreement with the CFD solutions in the vicinity of the shock at all of the chosen frequencies: 45, 100, and 200 Hz. This is because of the upstream boundary condition imposed in the solutions. As the solutions evolve downstream away from the shock, they deviate from each other significantly, especially at high frequencies. This is because the wave number is getting bigger as the frequency goes higher. As a result, the discrepancy in the wave number term, which is the main difference between the two models, is big enough to have a significant effect on the angle. Moreover, as the location is farther away from the shock, the discrepancy in the wave number is multiplied by the displacement away from the shock. This is the reason why the significant differences are shown clearly in the high-frequency range. There is some degree of undulation in the prediction from the theory at 45 Hz. Because the perturbation ε is largest at around 45 Hz, as shown in Fig. 5, the undulations in the solutions from the quasi-one-dimensional model come mainly from ε^2, the second-order effect. This comparison suggests that the weakly reflected wave model is a more appropriate model for this problem.

Before we move on to apply this model to solve the perturbed unsteady continuity equation (36), the physical meaning of the weakly reflected wave model is discussed.

The model assumes virtually no reflections as the disturbance $\Delta \boldsymbol{u}$ propagates upstream toward the shock. There are two mechanisms for a wave reflection to take place. The first one is when the disturbance hits the shock within the shock excursion range where the shock velocity is virtually zero compared with the local speed of sound. The second one occurs during the disturbance propagating upstream toward the shock against the outflow from the gradually narrowing nozzle.

As discussed for the dual-oscillator concept, for the first mechanism to create a reflected wave, according to the conservation of linear momentum, it is necessary for the subsonic disturbance to transmit a perturbed momentum upstream through the virtually stationary shock into the supersonic domain for a reverse in momentum, which is not possible. The shock moves to a new location in a manner associated with the phase angle to accommodate the influence from the change of the downstream pressure to the shock.

For the second mechanism to create a reflected wave, according to the linear theory of acoustics in a noncompact region,[16,18] which is the case for a gradually narrowing nozzle, the variation of the speed of sound, or/and the acoustic admittance or its gradient, in the streamwise direction must be significant relative to its local value. The acoustic admittance is a measure of the reciprocal of resistance or impedance and is defined as

$$Y = \frac{\text{volume flow in direction of propagation}}{\text{pressure excess}} \tag{58}$$

The speed of sound varies within 5% of its mean value and has in the worst case only one cycle in the subsonic domain. Its gradient relative to its local value is, therefore, insignificant. The variations of Y and its gradient in the subsonic domain are reasonably smooth except at the nozzle exit where the disturbance starts to propagate upstream toward the shock. Equally, the steep gradient of Y at the nozzle exit indicates that certain degree of wave reflection with a momentum equal and opposite to the entering external wave must have taken place there and is traveling downstream away from the nozzle exit. As a result, there is an abrupt change in ΔP at the exit, which will be implemented in the theory for the convective energy assessment at the exit. This abruptness or discontinuity in ΔP at the nozzle exit does not influence significantly the continuity of other flow parameters at the exit as shown by Lighthill[18] and Batchelor.[26]

To justify quantitatively the smoothness requirement on Y and its gradient in the streamwise direction, the following formula based on the linear acoustic theory[18] can be employed:

$$E = \tfrac{1}{2}\left[c_r'/c_r - \tfrac{1}{2}(Y'/Y) + Y''/Y'\right]Y'/Y(c_r/\omega)^2 \tag{59}$$

where E is a measure of the smoothness requirement and is $\ll 1$ for an insignificant wave reflection to take place inside a noncompact subsonic domain. In our problem, the most probable frequency for a significant wave reflection to take place inside the subsonic domain is at around 45 Hz, and E is ≈ 0.2.

Based on this linear acoustic theory, we can conclude that the existence of a reflected wave inside the subsonic domain is of a second order in magnitude, ε^2, which is in general small except in the resonance case at around 45 Hz. Here the second-order effect could be significant if ε is not $\ll 1$. It may be important for a nozzle designer to be aware that the existence of a strong wave reflection inside a subsonic domain increases significantly as a result of a significant value in E if the nozzle contour or its gradient is not smooth enough, or the nozzle angle is not shallow at all. These factors, among others, enhance the likelihood of creating an unwanted strong standing wave inside the nozzle. On the other hand, Eq. (59) shows that it is unlikely to have a strong reflection and, consequently, a strong standing wave at a high frequency, provided that the gradients of Y and c are small. In the experimental scale, these gradients may be not small and, hence, provoke a strong reflection to occur at a high frequency.

We are now in a position to solve the perturbed unsteady continuity Eq. (36). Substitution of Eqs. (38) and (43) into Eq. (36), in addition to the condition of a rigid wall such that $\partial \boldsymbol{A}/\partial t = 0$, yields a first-order perturbed unsteady continuity equation,

$$\frac{\partial \Delta\rho}{\partial t} + \boldsymbol{u}_0 \frac{\partial \Delta\rho}{\partial \boldsymbol{x}} + \rho_0 \left(\frac{\partial \Delta \boldsymbol{u}}{\partial \boldsymbol{x}} + \frac{\Delta \boldsymbol{u}}{\boldsymbol{A}} \frac{\partial \boldsymbol{A}}{\partial \boldsymbol{x}} \right) = 0 \tag{60}$$

where

$$\frac{1}{\boldsymbol{A}} \frac{\partial \boldsymbol{A}}{\partial \boldsymbol{x}} \approx \frac{d}{\boldsymbol{x}_0 + \boldsymbol{x}}$$

for a large area-ratio ($\gg 1$) nozzle. We shall employ the weakly reflected wave model, Eq. (55), for the perturbed velocity in Eq. (60),

which becomes

$$\frac{\partial \Delta\rho}{\partial t} + \boldsymbol{u}_0 \frac{\partial \Delta\rho}{\partial \boldsymbol{x}} = -\frac{2\omega \Delta \boldsymbol{x}_m \rho_{20}}{\gamma+1}\left[\sin(\omega t + \phi + \kappa \boldsymbol{x}) \frac{2\kappa \sin(2\kappa \boldsymbol{x})}{[1+(\boldsymbol{x}/\boldsymbol{x}_0)]^d} - \frac{d}{\boldsymbol{x}_0 + \boldsymbol{x}} \cos(\omega t + \phi + \kappa \boldsymbol{x})\right] + \mathcal{O}\left(\frac{\varepsilon}{M_{10}^2}, \varepsilon^2\right) \tag{61}$$

where κ and its space derivative are taken in a mean value form in this first-order estimation because $\Delta \boldsymbol{x}_m \sim \mathcal{O}(\varepsilon)$. The $\sin(2\kappa \boldsymbol{x})$ factor in the first term is to satisfy the boundary condition at the shock shown later, and the derivatives of $\Delta\rho$ are dominated by the second term. In addition, this factor together with the attenuation factor, $(1+\boldsymbol{x}/\boldsymbol{x}_0)^d$, take into account the variation of κ in space that controls the turning points of $\Delta\rho$ in space. This attenuation factor for κ is purely a consequence of changing in the cross-sectional area and has been observed and confirmed by CFD evaluations in the mean value of κ in the subsonic domain. In general, downstream away from the shock, $\kappa \boldsymbol{x}$ varies weakly with respect to time and space, and its derivatives can be regarded as a second-order effect.

From the continuity, momentum, and energy (20), (21), and (22), together with the condition of a constant mass flow rate in the supersonic regime, the upstream boundary condition of $\Delta\rho$ just behind the conical shock can be shown to be

$$\Delta\rho_2 = -\rho_{20}(\Delta \boldsymbol{A}_2/\boldsymbol{A}_{20}) + \mathcal{O}\left(\varepsilon \big/ M_{10}^2\right) \tag{62}$$

For a large area-ratio nozzle, Eq. (62) can be simplified as

$$\Delta\rho_2 \approx -(\rho_{20} d \Delta \boldsymbol{x}/\boldsymbol{x}_0) = (\rho_{20} d \Delta \boldsymbol{x}_m/\boldsymbol{x}_0)\sin(\omega t + \phi) \tag{63}$$

A first-order approximate solution to the Eq. (61), as $\boldsymbol{x} \ll \boldsymbol{x}_0$, is given by

$$\Delta\rho = \frac{2\omega \Delta \boldsymbol{x}_m \rho_{20}}{(\gamma+1)}\left\{\frac{2\sin(2\kappa \boldsymbol{x})}{(a-\boldsymbol{u}_0)(1+\boldsymbol{x}/\boldsymbol{x}_0)^d} + \frac{d\,\ell_n(1+\boldsymbol{x}/\boldsymbol{x}_0)}{\boldsymbol{u}_0}\right\} \times \cos(\omega t + \phi + \kappa \boldsymbol{x}) + \frac{\rho_{20} d \Delta \boldsymbol{x}_m}{\boldsymbol{x}_0}\sin(\omega t + \phi) \tag{64}$$

where a is the local speed of sound as defined by Eq. (46). Figure 8 shows a comparison of $\Delta\rho$ with the CFD results at the resonant frequency of 45 Hz. In general, the gradients of $\Delta\rho$ or phases from the theory are in reasonable agreement with the CFD prediction.

The perturbative stored energy inside the subsonic domain in one period of the cycle is given by

$$\Delta E_{s2} = \left[\int_0^L \left(\frac{\boldsymbol{u}^2}{2} + e\right)\rho \boldsymbol{A}\, \mathrm{d}\boldsymbol{x}\right]_0^{1/f} \tag{65}$$

where the difference of the stored energy at two different times separated by a period is evaluated and e is equivalent to $P/\rho(\gamma-1)$ for a perfect gas. Substitution of Eqs. (38), (55), (56), and (64), corresponding to the weakly reflected wave model, into Eq. (65) yields

$$\Delta E_{s2} = \mathcal{O}\left(\varepsilon^2 \big/ M_{10}^2, \varepsilon^3\right) \tag{66}$$

as expected intuitively because all of the perturbative parameters in the magnitude of $\mathcal{O}(\varepsilon)$ are found to be periodic from the theory. Nevertheless, all of the efforts to form $\Delta \boldsymbol{u}$, ΔP, and $\Delta\rho$ are not wasted because we shall need these equations to evaluate the convective energy due to the mass transfer through the control surfaces at the inlet and outlet of the control volume as shown later.

It can be concluded from this analysis that the energy storage for a cycle period within the defined control volume consists of mainly the energy dissipation through the periodic shock movement. For a cycle period, the subsonic domain contains no net energy storage and acts basically like an energy conveyer transferring the perturbative stored energy upstream and downstream between the shock and the external pressure at the nozzle exit.

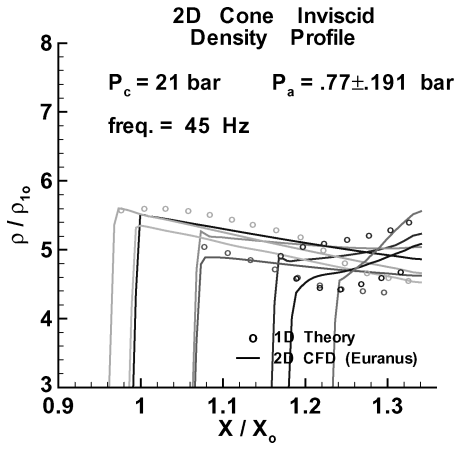

Fig. 8 Comparison of $\Delta\rho$ with a weakly reflected wave model.

B. Convective Energy

At the inlet of the control volume, the flow is supersonic and, hence, steady. For this reason, there is no contribution to the perturbative convective energy from the mass transfer through the control surface at the inlet.

At the outlet of the control volume, the convective power can be evaluated as

$$(E_c/m_3)\dot{m}_3 = \left\{[\gamma/(\gamma-1)](P_3/\rho_3) + \left(\boldsymbol{u}_3^2/2\right)\right\}\rho_3 \boldsymbol{A}_3 \boldsymbol{u}_3 \tag{67}$$

where E_c/m_3 is the specific convective energy at the nozzle exit. Substitution of the perturbative terms

$$P_3 = P_{30} + \Delta P_3, \qquad \boldsymbol{u}_3 = \boldsymbol{u}_{30} + \Delta \boldsymbol{u}_3, \qquad \rho_3 = \rho_{30} + \Delta\rho_3 \tag{68}$$

into Eq. (67), in addition to a time integration over a cycle period, yields the perturbative convective energy as

$$\Delta E_c = \int_0^{1/f} \frac{\gamma}{\gamma-1}\boldsymbol{A}_3 \Delta P_3 \Delta \boldsymbol{u}_3 + \frac{3}{2}\boldsymbol{A}_3 \boldsymbol{u}_{30} \times \left(\boldsymbol{u}_{30}\Delta \boldsymbol{u}_3 \Delta\rho_3 + \rho_{30}(\Delta \boldsymbol{u}_3)^2\right)\mathrm{d}t + \mathcal{O}\left(\frac{\varepsilon^2}{M_{10}^2}, \varepsilon^3\right) \tag{69}$$

The first term comes from the external pressure work that is associated with the internal energy in the convection. The second term is due to the interaction between the perturbed density and velocity, in which their relative phase difference plays an important role. This term determines the perturbative correlation between the mass flow rate and the specific kinetic energy. The third term comes from the perturbative kinetic energy in the convection.

We employ the solutions from the weakly reflected wave model, Eqs. (55), (56), and (64), for $\Delta \boldsymbol{u}_3$, ΔP_3, and $\Delta\rho_3$, respectively. ΔP_3 has acquired the correct phasing from the weakly reflected wave model, but its amplitude has to be adjusted by a factor of $\varepsilon_{30}/\varepsilon$ because of its discontinuity at the nozzle exit as discussed earlier. The solution of Eq. (69) becomes

$$\Delta E_c = \frac{2\pi\gamma}{\gamma^2-1}\frac{\varepsilon_{30}\dot{m}_0 \Delta \boldsymbol{x}_m}{M_{30}} \times \underbrace{\left[\frac{a_{20}\sin(\phi+\kappa L)}{\gamma} - \frac{8\pi}{\gamma+1}\frac{f\Delta \boldsymbol{x}_m \sin^2(\kappa L/2)}{\varepsilon}\right]}_{\text{external pressure work}} + \frac{3\pi}{\gamma+1}\dot{m}_0(\Delta \boldsymbol{x}_m)^2\left\{\frac{\boldsymbol{u}_{30} d \sin(\kappa L)}{\boldsymbol{x}_0} - \frac{4\pi f}{\gamma+1} \times \underbrace{\left[\frac{2a_{20}M_{30}\sin(2\kappa L)}{(a_{20}-\boldsymbol{u}_{30})s} + \ell_n(s)\right]}_{\text{density-velocity interaction}}\right\} + \underbrace{\frac{12\pi^2 f}{(\gamma+1)^2}\dot{m}_0(\Delta \boldsymbol{x}_m)^2}_{\text{kinetic energy}} + \mathcal{O}\left(\frac{\varepsilon^2}{M_{10}^2}, \varepsilon^3\right) \tag{70}$$

and

$$s = (1 + L/\boldsymbol{x}_0)^d \tag{71}$$

where ε_{30} and ε are the amplitudes in the pressure variation relative to the mean pressure (relative pressure amplitude) at the nozzle exit and at the shock, respectively. When the perturbative convective energy, Eq. (70), is compared with the perturbative stored energy, Eq. (35), it can be seen that the distance between the nozzle exit and the shock, L, and the Mach number in the subsonic domain play a significant role in the convective energy, but not at all in the stored energy in this inviscid theory.

C. Resonance and Damping

We are now in a position to sum up all of the perturbative energies considered earlier for one period of cycle. According to the principle of conservation of energy, the sum of the perturbative stored energy and the perturbative convective energy is zero. Hence,

$$\Delta E_s + \Delta E_c = 0 \tag{72}$$

From Eqs. (35) and (66), we learn that the perturbative stored energy is essentially the energy dissipated by the periodic shock motion. Equation (72), therefore, has the following implication: Any amount of gain in the energy dissipated by the periodic shock motion is compensated by the same amount of loss in the perturbative convective energy at the nozzle exit.

Because of the periodic terms in the perturbative convective energy, as shown in Eq. (70), this together with Eq. (72) lead us to deduce that, in the periodic shock motion, resonance takes place when the perturbative convective energy is a minimum, whereas damping occurs during the transition in the perturbative convective energy from a minimum to a maximum. This process of resonance and damping behaves like a Bessel function that is oscillatory with a diminishing amplitude as frequency increases. The diminishing amplitude of the periodic shock motion, $\Delta \boldsymbol{x}_m$, as frequency increases is attributed to the phase angle factor, $\cos(\phi)$, as shown in the shock displacement equations (28) and (29).

To confirm this deduction, we can substitute Eqs. (35) and (70) into Eq. (72) so that ε, the relative pressure amplitude at the shock, can be expressed in terms of ε_{30}, the relative pressure amplitude at the nozzle exit, as

$$\varepsilon = \frac{2\gamma}{\gamma - 1}\frac{\varepsilon_{30}}{M_{30}}\left(\left[\frac{-a_{20}\sin(\phi + \kappa L)}{\gamma \boldsymbol{x}_0(-\mathrm{GRP})\cos(\phi)} + \frac{8\pi f}{\gamma + 1}\sin^2\left(\frac{\kappa L}{2}\right)\right]\Bigg/ \times\left[\frac{3\boldsymbol{u}_{30} d\sin(\kappa L)}{\boldsymbol{x}_0} + 4\pi f\{2 + DV\}\right]\right) \tag{73}$$

where DV stands for the terms generated by the perturbative interaction and correlation between the density and the velocity and can be expressed as

$$\mathrm{DV} = \frac{3}{\gamma + 1}\left\{1 - \left[\frac{2a_{20}M_{30}\sin(2\kappa L)}{(a_{20} - \boldsymbol{u}_{30})s} + \ell_n(s)\right]\right\} \tag{74}$$

The first term in Eq. (74) represents the contribution from the perturbative kinetic energy, and the other terms come from the perturbative mass flow rate.

Equation (73) is plotted vs frequency as shown in Fig. 9, where the curve of pressure–velocity work represents the numerator of this equation and the curve of density–velocity interaction represents the denominator of the equation. It can be seen that the strong nonmonotonous variation of the DV term in Eqs. (73) and (74) determines the maxima and minima of ε, the relative pressure amplitude at the shock, which is shown in Fig. 10 vs the frequency. The top and bottom curves represent the variation of the relative pressure amplitude at the shock vs frequency with the relative pressure amplitudes of 0.09 and 0.045 at the nozzle exit, respectively. The bottom curve with a smaller relative pressure amplitude at the nozzle exit, showing a better agreement with the theory, suggests

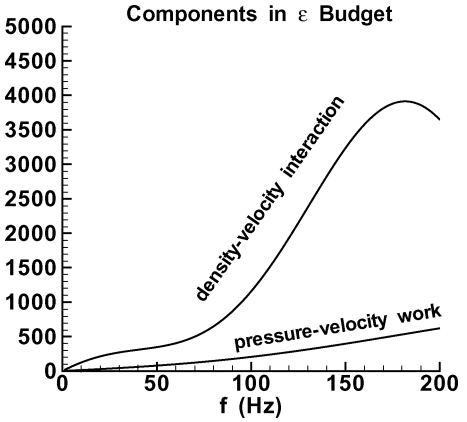

Fig. 9 Factors to determine ε budget against frequency.

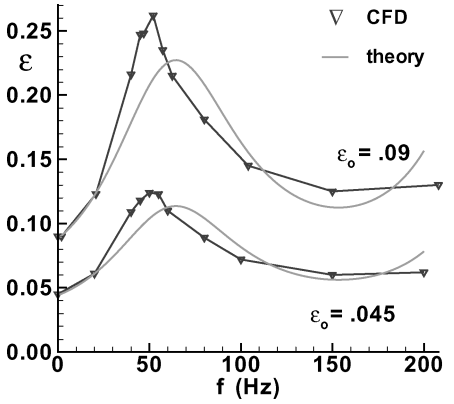

a) Relative pressure amplitude behind shock

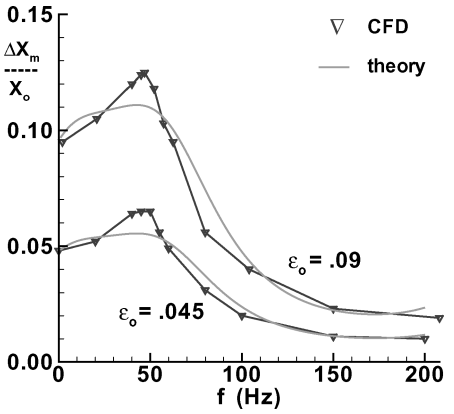

b) Shock maximum displacement

Fig. 10 Comparison between theory and CFD in amplification factor and shock excursion.

that the discrepancy between the theory and the CFD results is attributed mainly to the effect of the second-order terms ignored in the theory. The same remark is applied to the comparison between the theory and the CFD results in the shock excursion against frequency as shown in Fig. 10. Despite of the deficiency of the higher-order terms, the theory predicts the resonant frequency very close to those from the CFD results.

Based on this inviscid perturbative approach, it can be concluded that the phenomena of resonance (maximum) and damping (minimum) in the pressure amplitude just behind a periodic shock motion is a consequence of the corresponding loss and gain in convective energy in the subsonic outflow, which is governed mainly by the correlation between the compressibility and the flow velocity. Moreover, Eq. (73) shows that the amplification of the perturbed pressure behind shock, which is measured by the ratio $\varepsilon/\varepsilon_{30}$, is independent of the amplitude of the external pressure fluctuation. This result has a

significant influence on the experimental setup, pressure transducer measurement, and data evaluation because in practice it is very unlikely to have a constant amplitude of external pressure fluctuations at all frequencies as demonstrated by Torngren.[11]

IV. Range of Applicability

A. Areas

Nonlinear Oscillator

Only first-order terms are considered in the perturbative quasi-one-dimensional model presented. For a better accuracy in the prediction, second- or higher-order terms should be included in the analysis, but would be very tedious. Based on the first-order approach, the assumption of a periodic shock motion (linear oscillator) matches reasonably well with the CFD results. However, it is very probable that the oscillator is nonlinear in the second-order terms, which could become significant, especially for the case with a large cone angle. The oscillator sweeps across a divergent or convergent area in its periodic excursion along the cone axis of symmetry. The difference in the swept area between the two halves of a cycle in a periodic motion becomes significant as the cone angle increases.

Acceleration Effect

At a low frequency, the acceleration effect is still insignificant so that the maximum shock speed is one order of magnitude smaller than the upstream velocity just in front of the shock. At a high frequency, where the shock speed is comparable with the upstream velocity, the Galilean transformation application is no longer valid. It is important to make sure that the range of frequencies considered are within the shock speed limit applicable for this theory.

Viscous Effect

The significance of the viscous effect to the periodic shock motion could vary from case to case. It depends on, among other things, the vortex strength, the skin friction at the nozzle wall, the volume of the subsonic domain, and possibly the cone angle. These parameters affect the energy storage in the subsonic domain, which can then reduce the energy dissipation in the periodic shock motion according to Eq. (72). In general, it is appropriate to state that, the closer is the conical shock to the nozzle exit, the less influence is the viscous effect to the periodic shock motion. In the case where viscous effect is significant, this theory can still provide an upper bound estimation in the shock excursion.

In general, the energy transfer in the boundary layer upstream of the shock is relatively small compared with the energy storage in the subsonic domain downstream of the shock. The viscous effect upstream of the shock is, therefore, relatively less important to the periodic shock motion; however, it does affect the location of the conical shock but to an extent that is negligible compared to L or the shock excursion considered in this theory. This may be regarded as the Reynolds effect where turbulent shock-wave/boundary-layer interaction plays a major role. It is beyond the scope of this paper to discuss this interaction, and because the objective of this theory is not for the prediction of the location of the shock but rather its excursion due to the external pressure fluctuation, this kind of interaction is not considered as a critical issue for this theory, at least from the energy storage point of view.

In practice where viscous effect is significant, instead of using the standard table[20] for inviscid flows, one can extract the mean location of the conical shock, $\boldsymbol{x}_0$, from a CFD steady calculation with any classical turbulence model that can handle attached flow. In the case where the nozzle is nonconical, as will be discussed, the conical shock becomes a separation shock that is in general nonconical; the accuracy in the prediction of $\boldsymbol{x}_0$ from CFD, which is in general more difficult in a separation shock than in a conical shock, does influence the outcome of the prediction from this theory to a certain degree as shown in the S6 nozzle example to come.

Tangential Flows

This theory is based on a quasi-one-dimensional approach that does not take into account tangential flows perpendicular to the radial direction other than by changing the cross-sectional area along the cone axis. For a cone angle of 15 deg or less, the tangential flows can be regarded as a second-order effect. Beyond this cone angle limit, the theory has to be modified to accommodate the energy storage due to the tangential flows in the subsonic domain.

Nozzle End Effect

This effect is also known as incipient separation and takes place when the separation shock is close to the end of the nozzle. The separation pressure experiences an anomalous increase instead of a decrease that is normally the case with a larger local area ratio. In general, this theory is applied to a conical shock, and approximately to a separation shock, some distance upstream from the nozzle exit where the nozzle end effect can be ignored.

Other Effects

There are other important effects not considered in this theory such as the heat exchange through thermal conduction between the nozzle wall and fluids, the high-temperature effect to the flow properties, and the nozzle wall elasticity. These effects should be considered in a practical engine nozzle with hot flows. However, for an experimental nozzle with cold flows, such as those described in Refs. 11 and 21, where the nozzle size is scaled down, the thermal effects are insignificant.

The mechanical structure of a nozzle has a spectrum of discrete eigenmodes such as ovalization, pendulum, and bending described in Refs. 27 and 28, which interact with the flow-induced pressure fluctuation at the nozzle wall. This kind of aeroelastic instability could induce buckling and has a significant impact on the separation shock location, as well as on its response to external pressure fluctuations. It is beyond the scope of this quasi-one-dimensional theory to include this three-dimensional aeroelastic instability effect. This theory can be applied for validation purpose in unsteady flows, or as a parametric study in the nozzle design where the external pressure fluctuation is significant, provided that the aeroelastic instability is negligible under the flow condition considered.

In a three-dimensional nozzle configuration, any local disturbance, such as surface roughness, or asymmetric flow disruption from the plenum upstream of the shock could suppress entirely the azimuthal coherence of the unsteady flow. This can affect the wave reflectivity significantly.

Nonconical Nozzles

Conical nozzles have been employed in the past mainly as small thrusters in satellites, for example, the ERNO-0.5N thruster. However, a rocket engine nozzle that covers low and high altitudes is, in general, contoured to fulfill a competitive constraint in performance efficiency. A contoured nozzle can be of many shapes, such as truncated ideal contour (TIC) or thrust optimised contour (TOC), depending on the design criteria. In general, a contoured nozzle has a much more complex flowfield than the conical shock from a conical nozzle, as discussed by Frey.[29]

In the FSS case in an overexpanded TIC nozzle where there is a Mach disk in the center of the core flow, as a first-order approximation in terms of the energy storage, this theory can still be applied to the subsonic domain behind the separation shock and the Mach disk. As mentioned earlier for the viscous effect, for a better prediction in the shock excursion, it is necessary to estimate how much energy is stored in this subsonic domain due to the circulation flow behind the separation shock. The energy convected by the relatively small volume of supersonic jet as a result of the shock and shear-layer interaction is assumed relatively insignificant and can be regarded as a second-order contribution to the energy budget. With exclusion of this viscous effect, which is in practice difficult to estimate, this theory can still provide an upper bound estimation in the shock excursion due to the external pressure fluctuation at the nozzle exit.

Similar treatment can be applied to the RSS case, for example, in the Volvo S1 parabolic nozzle,[21] where there is a trapped vortex in the core flow, and adjacent to it, massive shock-wave/boundary-layer and shock-wave/shear layer interactions close to the nozzle wall. The theory can not evaluate the amount of energy consumed

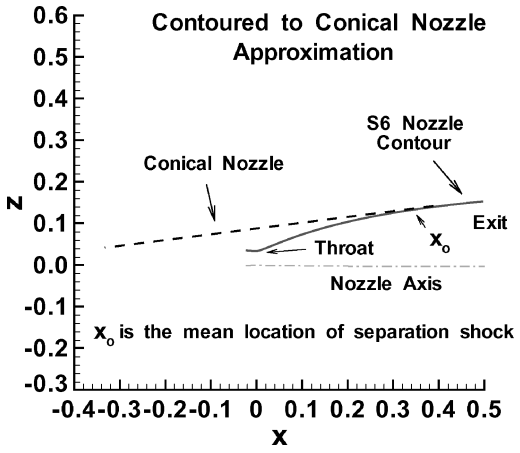

Fig. 11 Contoured nozzle approximation.

in these interactions but is able to provide an upper bound estimation in the shock excursion, provided that these interactions take place in a relatively small volume of the flow.

Before one can apply this theory to a contoured nozzle, it is necessary to convert the nozzle to a conical nozzle for a correct estimation of the mean separation shock location $\boldsymbol{x}_0$ relative to the throat of a conical nozzle, as shown in Fig. 11. A tangent is drawn at $\boldsymbol{x}_0$ to the contoured nozzle and extended upstream to the location with the same throat radius as the contoured nozzle. This is an important approximation to relate the area ratio in a contoured nozzle to the same area ratio in a conical nozzle.

The accuracy in the prediction from this theory is very sensitive to the accuracy of the input data that represent the mean flow characteristics. This is especially important for the case of flow separation with reverse flows, which in general have the significant effect of reducing the mean velocity $\boldsymbol{u}_{30}$ and the mean Mach number M_{30} at the nozzle exit. Equation (73) indicates that a lower value in both $\boldsymbol{u}_{30}$ and M_{30} renders a larger pressure amplification behind shock and, consequently, a larger shock excursion. In other words, the flow separation with reverse flows has a tendency to drive and promote the oscillations of the shock. This shows the same conclusion as by Culick and Rogers[14] for the response of normal shocks in diffusers.

B. Example of S6 Contoured Nozzle

This is a TIC nozzle with a Mach disk in the center of the core flow and an oblique separation shock inclined to the nozzle wall under an ideal FSS condition. Full details of the nozzle can be found by Torngren.[11] It has a shallow exit wall angle and can be approximated as a conical nozzle as mentioned earlier and shown in Fig. 11.

We shall compare the prediction from the theory with the CFD solutions recently published[30] and with the experimental data.[11] Note that the CFD solutions are based on the S6 contoured nozzle from the experiment[11] but include an extension that scales up to 0.5 m from the throat of the nozzle. We adopt the configuration from the CFD because a steady-state solution without any external pressure fluctuation is required for the input condition in the theory. The experimental data can be scaled by the theory, which takes into account the parameters that determine the shock displacement, $\Delta \boldsymbol{x}_m$, as shown next.

The following input data for the theory are based on CFD steady-state solutions under the external pressure 0.77-bar condition as stated in Ref. 30 but without any external pressure fluctuation:

1) The mean location of the separation shock, $\boldsymbol{x}_0$, is $\approx$0.35 m, which is equivalent to 0.70 m from the throat of the conical nozzle.

2) The separation length L is 0.15 m.

3) The mean upstream velocity $\boldsymbol{u}_{10}$ is 770 m/s.

4) The GRP factor, for $M_{10} \approx 5$, is -0.7.

5) The mean exit velocity $\boldsymbol{u}_{30}$ is 200 m/s.

6) The mean speed of sound behind shock, a_{20}, is 340 m/s.

7) The relative amplitude of the pressure fluctuation at the exit, ε_{30}, is 0.09.

8) The mean Mach number at the exit, M_{30}, is 0.6.

The experimental data for shock excursion are rather crude because they have been obtained from just one typical cycle of the shock movement. Torngren[11] measured the shock excursion only at one frequency, 150 Hz, which, for a pressure ratio (reservoir against ambient) of $\approx$27, is the largest shock excursion out of the range of frequencies (40–300 Hz) that have been measured in terms of pressure correlations between two transducers where one is located behind the shock and the other one is outside the nozzle in the freestream. Moreover, the experiment excites a pressure fluctuation of 6% in the freestream instead of 10% of the ambient pressure as taken in the CFD calculation. In the input data, we have taken 9% to take into account the drop in the amplitude of the mean pressure fluctuation from the freestream to the nozzle exit, as predicted in the CFD calculation.

To extrapolate the experimental data to the CFD condition, it is necessary to recall the theory in the induced shock motion, where the shock displacement is given by

$$\Delta \boldsymbol{x}_m / \boldsymbol{x}_0 = -\varepsilon \cos(\phi)(\text{GRP}) + \mathcal{O}(\varepsilon^2)$$

where ε is linearly proportional to the relative amplitude of the pressure fluctuation at the nozzle exit, ε_{30}, as shown in Eq. (73). For a pressure ratio of $\approx$27, the factors in parentheses, GRP, are approximately the same for both cases because $M_{10}^2 \gg 1$ as shown in the shock movement equation (27). Hence, the experimental data should be adjusted by the factors corresponding to the change in ε, $\boldsymbol{x}_0$, and $\cos(\phi)$. The first factor of adjustment is, therefore, approximately the ratio of the relative amplitude of the pressure fluctuation at the nozzle exit, which is 0.09/0.06. The mean location for the separation shock in the experiment is $\approx$0.21 m, which corresponds to a distance of $\approx$0.35 m from the throat of a conical nozzle. Hence, the second factor of adjustment is 0.7/0.35. The adjustment due to the $\cos(\phi)$ factor can be evaluated from Eq. (29) for the phase angle, which results the third factor of adjustment to be 1.16/1.56. The shock excursion from Ref. 11 at 150 Hz is estimated to be 21 mm, which is extrapolated to $\approx$45 mm after the three adjustment factors from the theory to fit with the CFD nozzle conditions.

Figure 12 shows a comparison among the theory, CFD, and experimental data (extrapolated). The other experimental data excluding 150 Hz, are based on the change in the pressure correlation relative to the one at 150 Hz and extrapolated in the same way as in the 150-Hz case.

In general, the comparison between the theory and the experimental data is as expected. The relatively larger discrepancy at higher frequencies is mainly due to the acceleration effect as discussed earlier. The shock excursion from the experimental data is generally smaller than that predicted by the theory and could be attributed to the loss in energy storage because of the ignored viscous effect in the theory, which includes turbulence and circulation of vortices in the subsonic domain. In addition, there is some energy lost due to shock and shear layer interactions. As a result, the energy dissipation due to the separation shock motion is smaller than that predicted by the theory. However, there is still some uncertainty in the level of discrepancy (10–15%) because of the rather crude experimental data currently available.

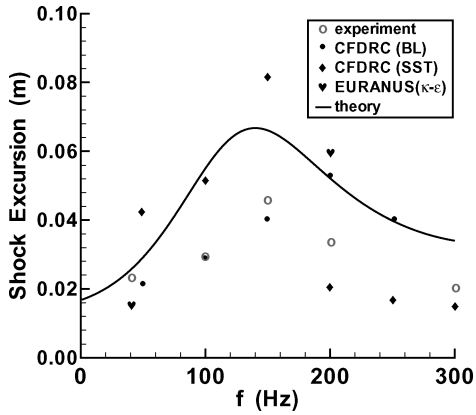

Fig. 12 S6 shock excursion against frequency.

A deficiency of accuracy in the assessment of turbulence effect in unsteady flows may be the main reason for the discrepancy between the experimental and CFD results as shown in Fig. 12.

The success of this theory lies in the use of the principle of conservation of energy to asssess the amount of energy dissipated by the induced separation shock motion. It would have been a lot harder to tackle this problem initially by resolving the fluid dynamics of the complex flowfield of shock and shear layer interactions that take place in a relatively small portion of the core flow. The failure of the theory in the assessment of the viscous effect renders a discrepancy between the theory and the experimental data.

Finally, the accuracy in the prediction of the separation shock motion due to external pressure fluctuations from this engineering method depends very much on how reasonable and accurate the input data are of the mean flow for the theory, which are usually acquired by CFD methods, in addition to the degree of deviation in the flow structure compared with the simple inviscid conical shock.

V. Conclusions

A perturbative quasi-one-dimensional model coupled with a dual-oscillator concept for unsteady conical or, to a certain extent, contoured nozzle flows has been established. It has been validated by CFD and experiments to predict an induced periodic shock motion, accurately in the case of a conical nozzle and reasonably well in the case of a contoured nozzle, as a result of external pressure fluctuations.

Resonance and damping in the pressure amplitude behind shock due to the external pressure fluctuation have been investigated and physically explained with some feasible mechanisms to identify the source of these effects. It has been shown that the standing wave (strong resonance) in the transonic case is a consequence of superimposing two azimuthal coherent, almost identical in amplitude but in opposite direction, traveling waves through the subsonic domain inside the separated boundary layer. In the supersonic or hypersonic case, a relatively weak resonance has been encountered as a result of the phasing in the convective energy transported between the energy dissipation due to the shock movement and the energy supply due to external pressure fluctuations. The damping effect comes mainly from the interaction and correlation between compressibility and velocity in the subsonic domain downstream of the shock.

The applicability of this theory can range from as a basis of interpretation of experimental and CFD results to a rapid but crude assessment of eigenfrequencies where resonance of a separation shock motion may occur in a conical or contoured nozzle. In addition, the theory provides deep insight on the influence of a large number of physical and geometrical parameters in the design of nozzle flow measurements.

It has to be stressed that this theory is not to replace other more sophisticated and reliable methods such as CFD or experiment in a wind-tunnel facility to predict or measure the induced shock excursion or its resonance due to external pressure fluctuations. On the contrary, this kind of engineering approach is to support them to narrow the range of frequencies that these methods can work in to search for the physical phenomena that are difficult to measure and predict accurately.

Prediction of flow separation and its unsteady motion in a general practical engineering nozzle hitherto has been still more like an art than a science because of its complexity with a vast number of physical phenomena, which are either crudely understood or difficult to measure or poorly estimated. It is hoped that this paper can help to take a step closer toward the asymptote of accurate engineering assessment of the sophisticated but important physics in unsteady nozzle flow separation.

Acknowledgments

The author gratefully acknowledges the support and encouragement from the colleagues in the European Space Technology and Research Center, especially R. Schwane, William Kordulla and Jean Muylaert. A part of the work presented in this paper has been performed within the framework of the European FSCD Working Group. The author is deeply indebted to the flow separation control device (FSCD) colleagues for many fruitful discussions and valuable comments.

References

[1]Hill, W., and Greene, P., "Increased Turbulent Mixing Rates Obtained by Self-Excited Acoustic Oscillations," *Journal of Fluids Engineering*, Vol. 99, 1977, pp. 520–525.

[2]Krothapalli, A., and Hsia, Y., "Discrete Tones Generated by a Supersonic Jet Ejector," *Journal of Acoustic Society America*, Vol. 99, 1996, pp. 777–784.

[3]Mabey, D., *Physical Phenomena Associated with Unsteady Transonic Flows*, Progress in Astronautics and Aeronautics, Vol. 120, AIAA, Washington, DC, 1989, Chap. 1, pp. 1–56.

[4]Schwane, R., Wong, H., and Torngren, L., "Validation of Unsteady Turbulent Flow Predictions for Over-Expanded Rocket Nozzles," *Proceedings of International Conference in CFD2*, Springer-Verlag, Berlin, 2002, pp. 707–712.

[5]Culick, F., "Oscillatory and Unsteady Processes in Liquid Rocket Engines," *Proceedings of Combustion Instability in Liquid Rocket Engines*, ESA Rept. WPP-062, Noordwijk, The Netherlands, Sept. 1993.

[6]Zaman, K., Dahl, M., Bencic, T., and Loh, C., "Investigation of a 'Transonic Resonance' with Convergent–Divergent Nozzles," *Journal of Fluid Mechanics*, Vol. 463, 2002, pp. 313–343.

[7]Hunter, C., "Experimental, Theoretical, and Computational Investigation of Separated Nozzle Flows," AIAA Paper 98-3107, July 1998.

[8]Sajben, M., and Kroutil, J., "Effects of Initial Boundary-Layer Thickness on Transonic Diffuser Flows," *AIAA Journal*, Vol. 19, No. 11, 1980, pp. 1386–1393.

[9]Loh, C., and Zaman, K., "Numerical Investigation of Transonic Resonance with a Convergent–Divergent Nozzle," *AIAA Journal*, Vol. 40, No. 12, 2002, pp. 2393–2401.

[10]Terhardt, M., Hagemann, G., and Frey, M., "Flow Separation and Side-Load Behaviour of the Vulcain Engine," AIAA Paper 99-2762, June 1999.

[11]Torngren, L., "Correlation Between Outer Flow and Internal Nozzle Pressure Fluctuations," *Proceedings of the 4th European Symposium on Aerothermodynamics for Space Vehicles*, ESA, Noordwijk, The Netherlands, 2001, pp. 415–424.

[12]Hussain, A., and Hasan, M., "The 'Whistler-Nozzle' Phenomenon," *Journal of Fluid Mechanics*, Vol. 134, 1983, pp. 431–458.

[13]Tijdeman, H., "Investigation of the Transonic Flow Around Oscillating Aerofoils," National Aerospace Lab., Rept. TR-77-090U, Amsterdam, 1977.

[14]Culick, F., and Rogers, T., "The Response of Normal Shocks in Diffusers," *AIAA Journal*, Vol. 21, No. 10, 1983, pp. 1382–1390.

[15]Sajben, M., "Comment on 'The Response of Normal Shocks in Diffusers,'" *AIAA Journal*, Vol. 23, No. 3, 1985, pp. 477, 478.

[16]Reynolds, D., *Engineering Principles of Acoustics*, Allyn and Bacon, Boston, 1981, pp. 2–5, 200–210.

[17]Landau, L., and Lifshitz, E., *Fluid Mechanics*, Course of Theoretical Physics, Vol. 6, Pergamon, Oxford, England, U.K., 1982, pp. 88–90, 263.

[18]Lighthill, J., *Waves in Fluids*, Cambridge Univ. Press, London, 1979, pp. 77–78, 92–95, 100–128.

[19]Nixon, D., *Unsteady Transonic Aerodynamics*, Progress in Astronautics and Aeronautics, Vol. 120, AIAA, Washington, DC, 1989, Chaps. 1, 2, pp. 13, 71.

[20]"Equations, Tables, and Charts for Compressible Flow," NACA Rept. 1135, 1953.

[21]Östlund, J., Damgaard, T., and Frey, M., "Side-Load Phenomena in Highly Overexpanded Rocket Nozzles," AIAA Paper 2001-3684, Aug. 2001.

[22]Eliasson, P., and Nordström, J., "The Development of an Unsteady Solver for Moving Meshes," Aeronautical Research Inst. of Sweden, Rept. FFA TN 1995-39, Stockholm, 1995.

[23]Jameson, A., "Time Dependent Calculations Using Multigrid, with Applications to Unsteady Flows Past Airfoils and Wings," AIAA Paper 91-1596, June 1991.

[24]Wang, D., Wallin, S., Berggren, M., and Eliasson, P., "A Computational Study of Unsteady Turbulent Buffet Aerodynamics," AIAA Paper 2000-2657, June 2000.

[25]Moody, F., *Introduction to Unsteady Thermo Fluid Mechanics*, Wiley, New York, 1990, pp. 30–34, 294–298.

[26]Batchelor, G., *An Introduction to Fluid Dynamics*, Cambridge Univ. Press, London, 1981, pp. 380–383.

[27]Tuovila, W., and Land, N., "Experimental Study of Aeroelastic Instability of Overexpanded Rocket Nozzle Extensions," NASA TN D-4471, 1968.

[28]Brown, A., "Characterization of Side-Load Phenomena Using Measurement of Fluid Structure Interaction," AIAA Paper 2002-3999, Aug. 2002.

[29]Frey, M., and Hagemann, G., "Flow Separation and Side-Loads in Rocket Nozzles," AIAA Paper 99-2815, July 1999.

[30]Schwane, R., Perigo, D., and Xia, Y., "Unsteady Numerical Simulations of the Flow in a Truncated Ideal Contour Nozzle Under Free Shock Separation Conditions," AIAA Paper 2003-3676, Aug. 2003.